Journal of Engineering Science and Technology
Vol. 21, No. 2 (2026) 541 - 549

EFFECTS OF IRON (III) OXIDE AND SINTERING TEMPERATURE ON THE PROPERTIES OF CLAY FOR VITRIFIED CLAY PIPE APPLICATION

NORADILA A. LATIF[1], SHARIFAH ADZILA[1,*], NADIA JASMIN[1], LIM S. HOOI[2], JOSEPH TAN[2]

[1]Faculty of Mechanical and Manufacturing Engineering, Universiti Tun Hussein Onn Malaysia, 86400, Batu Pahat, Johor, Malaysia
[2]JPC INTAN Sdn. Bhd. (Claytan Group), 57th Mile, Jalan Johor, 86100, Ayer Hitam, Johor, Malaysia
*Corresponding Author: adzila@uthm.edu.my

Abstract

The Vitrified Clay Pipe (VCP) is a ceramic material that has been widely used in the last century to build sanitary sewer pipelines. The high sintering temperature in Vitrified Clay Pipes (VCPs) has resulted in high energy consumption during the VCP manufacturing process. The mechanical strength, which is influenced by the sintering process, is also a crucial factor in VCP performance. This study investigated the properties of clay and clay reinforced with Iron (III) Oxide (Clay/Fe_2O_3) at various weight percentages from 5 wt.% to 25 wt.%. The properties of clay and Clay/Fe_2O_3 composites were also investigated at different sintering temperatures from 950 °C to 1120°C. The maximum shrinkage was 7.93% at a 75/25 clay/Fe_2O_3 ratio sintered at 1120 °C. The Modulus of Rupture (MOR) was also increased with sintering temperature. The maximum MOR of 45.54 MPa was exhibited at 80/20 Clay/Fe_2O_3 ratio sintered at 1120 °C. The shrinkage and the MOR results were in line with the microstructure obtained through Scanning Electron Microscopy (SEM) analysis. X-ray diffraction (XRD) analysis indicated that the main components of Clay/Fe_2O_3 composite were quartz, muscovite, and hematite phases. The study's findings suggest that Iron (III) Oxide (Fe_2O_3) has the potential to significantly improve the properties of clay for VCP application at lower sintering temperatures, thereby reducing energy consumption in the VCP manufacturing industry.

Keywords: Clay, Iron (III) Oxide, Modulus of rupture, Sintering, Vitrified clay pipe (VCP).

1. Introduction

The Vitrified Clay Pipe (VCP) has been widely used in the last century to build sanitary sewer pipelines. Clay pipes have been developed for approximately 6,500 years, while VCP, a newer generation of these pipes, has been utilised for around 200 years. Over 5 billion linear feet (1,524 billion meters) of VCPs have been installed in the USA due to their high corrosion resistance across the entire pH range, which is primarily used in sanitary and combined sewer systems [1].

Besides corrosion resistance, VCPs are strong and resistant to internal abrasion and external chemical attacks, heat-resistant, and non-conductive. VCPs have excellent resistance to static and dynamic pressure, as they are composed of rigid material and are not susceptible to the problems of deflecting or flattening under pressure. The clay pipes are physically inherent, so their properties remain constant for a long time [2]. VCPs are manufactured by blending a mixture of crushed clays, grog, and feldspar, extruding into a pipe shape, drying at 120-150 °C, and then firing to a temperature of almost 1100-1200 °C to give a glassy finish on a pipe.

Clay and grog are key ingredients in sewer pipe manufacturing. The function of clay is to ensure enough plasticity for the body to be shaped. Grog contains a non-plastic meta kaolinite upon firing clays above 800 °C. Feldspars are known as fluxing agents used in ceramic industries. Feldspars are usually utilised due to their alumina and alkali content. Feldspars consist of potassium and sodium as minor elements besides their SiO_2 and Al_2O_3 content. Despite the many advantages of VCPs, there are still some negative aspects to this pipe, such as its brittleness. Clay pipelines are susceptible to root intrusion, leading to wastewater blockages or leaks beneath [3].

Previous researchers have studied and reported Iron (III) Oxide (Fe_2O_3) in various applications. Preparation and research of these magnetic particles have recently been focused on nanoparticles due to their interesting optical, magnetic, electrical, and catalytic properties and are widely applied in magnetic fluids, biomedical applications, and the remediation of oil spills [4]. Fe_2O_3 nanoparticles have been used as an additive in the MgO-CaO mixture for refractories due to their inexpensive and convenient material [5].

On the other hand, Fe_2O_3 has been applied as an encapsulated material to modify bentonite clay and activated carbon into beads by biopolymer sodium alginate for the removal of cationic (lead and cadmium) and anionic (arsenic) toxic pollutants from an aqueous environment [6]. Advanced research on clay and Fe_2O_3 was continued by mixing with graphene oxide (GO) for the adsorptive removal of methylene blue dye from wastewater [7].

Thus, the studies of incorporation of Fe_2O_3 in clay have been abundantly reported for environmental applications [8-10], for example, in photodegradation for water treatment [11], sanitary and ceramic tiles [12]. To date, there is no study conducted on clay/Fe_2O_3 composite for VCP in sewerage applications. In Malaysia, the VCP is used for sewerage applications in most construction industries and urban development. The modulus of rupture (MOR) of the VCP averages around 31% at a sintering temperature of 1120 °C, while the shrinkage averages around 5.2% at the same sintering temperature. Most of the VCP industries want to reduce the cost of energy used in the manufacturing process and, at the same time, improve the MOR property.

This study aims to improve the MOR at low sintering temperatures to reduce the energy consumption in the VCPs manufacturing process. The need for reducing energy consumption in the manufacturing of VCPs is a pressing issue, and this study represents a significant step towards addressing it. The novelty of this study is a worthwhile contribution to the improvement of clay, which has not been studied until now.

2. Materials Preparation, Characterisation and Testing

2.1. Materials preparation

The clay materials were collected from the VCP industry (JPC-Intan Sdn. Bhd, (Claytan Group Malaysia). The clay consisted of 83% raw clay and 17% grogs. Iron Oxide (Fe_2O_3) powder was purchased at HmbG Chemicals, CAS number: 1308-37-1; 159.69 g/mol assay with a purity of 85.9%. The weight percentage (wt.%) ratio of clay (matrix) to Fe_2O_3 (reinforcement) is designed as shown in Table 1. The samples were designed as CF0 to CF25, which represent the weight percentage of Fe_2O_3 from 0 wt.% - 25 wt.%.

Table 1. Designation of weight percentage (wt.%) ratio of clay and Fe_2O_3.

Samples name	Clay (wt.%)	Fe_2O_3 (wt.%)
CF0	100	0
CF5	95	5
CF10	90	10
CF15	85	15
CF20	80	20
CF25	75	25

The clay was crushed into fine powder and mixed with Fe_2O_3 powder at different weight percentages based on Table 1. This process was carried out in a rotary ball mill at 100 rpm for 4 hours. The existing clay and Clay/Fe_2O_3 powders were carefully sprayed with water for the deagglomeration and humidifying process. The preparation of the ceramic samples (65 × 12 × 7 mm) is based on the three-point bending test according to ASTM C674-77, where 10g of powder was precisely uniaxially pressed at 40 MPa. The samples were then dried at 120 °C for 24 hours. The sintering process was set at 950 °C, 1000 °C, 1050 °C, 1100 °C and 1120 °C in the electrical furnace for 2 hours (in an air atmosphere) using a heating and cooling rate of 5 °C/min.

2.2. Samples characterization and testing

The firing shrinkages were calculated as Eq. (1)

$$\text{Firing Shrinkage (\%)} = \frac{L1-L2}{L1} \times 100\% \quad (1)$$

where *L1* and *L2* denote the as-casting and fired sample lengths, respectively, in millimetres. The MOR was determined and evaluated as a function of sintering temperature and Fe_2O_3 composition.

The MOR was obtained by the three-point bending test based on ASTM C674-77 [13]. The flexural strength was analysed in a three-point bending test temperature in a pneumatic press. The average MOR value was taken from three

samples for every parameter. The equation used to measure the flexural strength at three points is shown in Eq. (2)

$$\text{MOR (MPa)} = \frac{3PL}{2ah^2} X\ 100\% \quad (2)$$

where P is the load achieved at the failure time (N), a and h are the width and height of the specimen, respectively, in mm.

The identification of the crystalline phases in sintered clay and Clay/Fe_2O_3 samples was a comprehensive process, involving multiple steps and thorough analysis. The sintered samples were analysed under X-ray diffraction (XRD) (Bruker D8 Advance, using Cu-Kα radiation). The instrument operated at voltage and current settings of 30 kV and 40 mA, respectively, and used Cu-Kα radiation (λ=0.15406 nm). XRD diagrams were recorded in 2θ=10°- 90° at a step size of 0.02° for qualitative analysis.

The fractured surface of the samples was then examined under a Scanning Electron Microscope (SEM) (JEOL). The ruptured surface was analysed after the 3-point bending test on samples sintered at 1120 °C for clay (CF0) and clay with 20% Fe_2O_3 (CF20) due to the better mechanical performance of CF20 at this temperature and composition. The samples were sputtered and coated with gold before SEM analysis, ensuring a thorough examination of the samples.

3. Results and Discussion

Figure 1 depicts the shrinkage percentage of clay and clay reinforced with Fe_2O_3 at various weight percentages sintered at 950 °C to 1120 °C. The data show that the clay and Clay/ Fe_2O_3 composites exhibit linear increments of shrinkage with sintering temperature. CF20 and CF25 show higher shrinkage compared to CF0 when sintered at 1050 °C and above. Notably, the maximum shrinkage of 7.93% was achieved by CF25 (25% of Fe_2O_3) reinforcement in clay sintered at 1120 °C, highlighting the significant role of Fe_2O_3 in enhancing shrinkage.

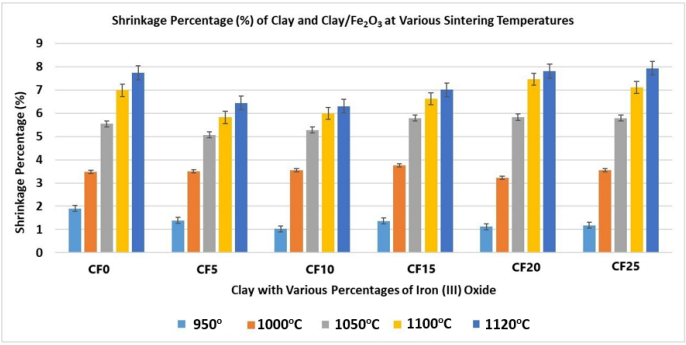

Fig. 1. Shrinkage percentage (%) of clay and Clay/Fe_2O_3 in various weight percentages at different sintering temperatures.

Figure 2 presents the MOR of clay and Clay/Fe_2O_3 composites sintered at 950 °C to 1120 °C. The MOR of Clay (CF0) and Clay reinforced with Fe_2O_3 (CF5, CF10, CF15) increases until 1100 °C and drops at 1120 °C. However, the MOR of CF20 and CF25 shows a linear increase with sintering temperature until 1120 °C.

The maximum MOR of 45.54 MPa is achieved at CF20 (20% Fe_2O_3 reinforcement) when sintered at 1120 °C. The obtained MOR is comparable to the MOR from the VCP industry, which is between 30-40 MPa at 1120 °C. CF5, CF15, CF20 and CF25 achieved MOR above 30 MPa when sintered at 1050 °C. The decrease in MOR between 1000 °C and 1120 °C might be due to the increase in porosity resulting from air expansion in the closed pores. A previous study by Alves et al. [13] reported the MOR of 25 MPa for kaolin clay sintered at 1300 °C, which is lower than the MOR of clay sintered at 1120 °C in this study.

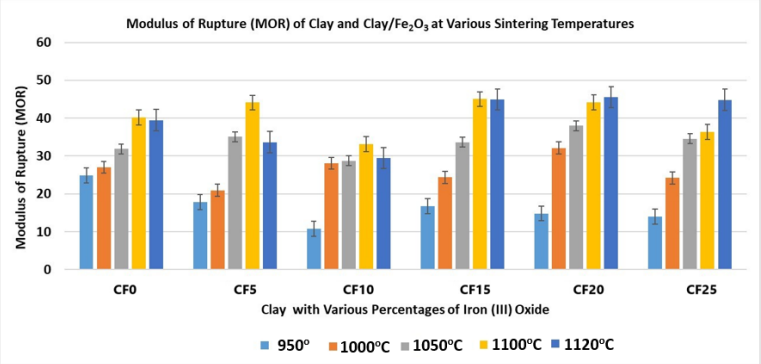

Fig. 2. Modulus of rupture (MOR) of clay and Clay/Fe_2O_3 in various weight percentages at different sintering temperatures.

Table 2 presents a comparison of shrinkage and MOR of clay with varying weight percentages of Fe_2O_3, sintered at 1120 °C. CF20 and CF25 exhibit the increment of the shrinkage and MOR, where the increase in shrinkage affected the MOR of clay with Fe_2O_3 at 20 wt.% and 25wt.%. The increase in shrinkage has reduced the pores, as shown in Fig. 2, and increased the MOR [12].

Table 2. Comparison of shrinkage (%) and MOR (MPa) of clay with various weight percentages of Fe_2O_3 sintered at 1120 °C.

Sample /Properties	Shrinkage (%)	MOR (MPa)
CF0	7.74	39.49
CF5	6.44	33.67
CF10	6.30	29.46
CF15	7.01	44.99
CF20	7.81	45.54
CF25	7.93	44.84

The X-ray diffraction (XRD) graph of clay and Clay/Fe_2O_3 composites sintered at 1050 °C, shown in Fig. 3(a), reveals intriguing findings. All the sintered samples contained the crystalline phases of quartz (SiO_2) and muscovite ($(KAl_2(AlSi_3O_{10})(FOH_2)$). The hematite phases ($Fe_2O_3$) are detected at CF5 until CF25. According to the theory proposed by Varela et al. [14], the mineral quartz (SiO_2), which is also known as silica, plays a crucial role in increasing mechanical strength and decreasing firing shrinkage, acting as a "skeleton" during the liquid phase formation. The existence of muscovite increases and becomes more visible after sintering at 1120 °C. The increase in quartz and muscovite phases with the composition of hematite is a particularly intriguing aspect.

Hematite helps the migration of particles within the liquid phase at high temperature due to the melting nature of Fe^{3+} increases a glassy phase after cooling [12]. The same trends were also similar to samples sintered at 1120 °C as shown in Fig. 3(b). Alves et al. [13] have also found that the XRD analysis of the raw clay shows quartz, which is the main constituent phase present in kaolin clay. The main components of clay in ceramic manufacturing are known as muscovite (illite or sericite), which is the micaceous clay mineral consisting of potassium in the crystal structure [15, 16]. Muscovite can exist generally with quartz (0-60 wt.%) and sometimes feldspars (0-30 wt.%), with variable proportions of other minerals, such as calcite, dolomite, iron and titanium oxides [17].

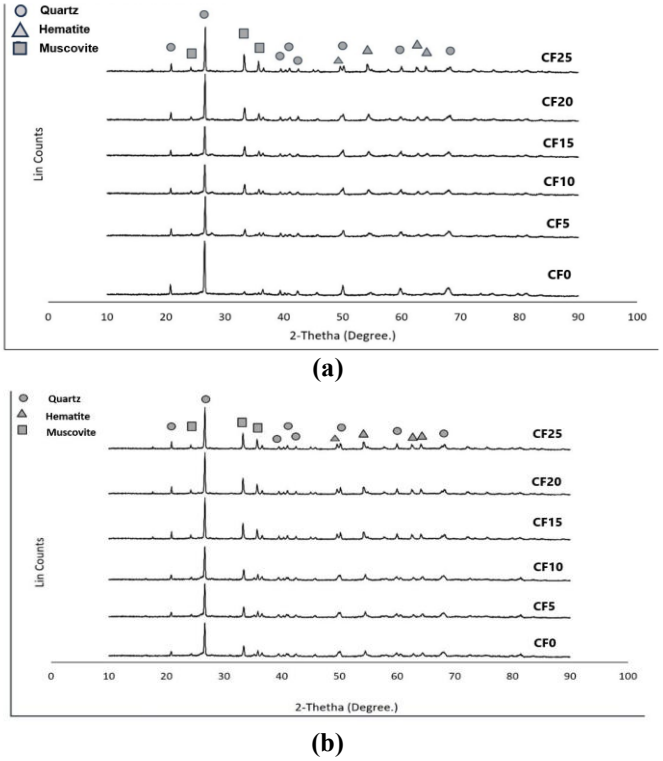

Fig. 3. XRD graph of clay and Clay/Fe_2O_3 composites sintered at; (a) 1050 °C and (b) 1120 °C.

Figures 4(a) and 4(b) show the fractured surface of CF0 and CF20 sintered at 1120 °C, respectively. The microstructure shows that the pores still existed on the fracture surface at 1120 °C. CF20 indicates that the pores are almost invisible when sintered at 1120 °C. Fe_2O_3 reinforcement aids in the sintering process of clay by reducing the pores, and this is similar to previous studies, which found the illite-kaolinitic clays with quartz and hematite [18, 19]. Martínez et al. [20] reported that the clay samples contained illite, chlorite, and kaolinite. The existence of carbonates (calcite and dolomite minerals) also leads to the formation of a porous structure due to the decomposition of carbonates by CO_2 during heating [20]. Thus, in this study, the increase of muscovite after sintering at 1120 °C from XRD analysis affected the microstructure that can be

related to the shrinkage and maximum strength (MOR) obtained from CF20, which resulted in higher shrinkage (7.93%) and a maximum MOR (45.54 MPa) compared to clay without reinforcement.

Dehsheish et al. [5] reported that Fe_2O_3 contribution in the matrix composite helps to form low melting point phases, improve the sintering mechanism by liquid phase, and decrease porosities and grain boundaries. The Fe_2O_3 might infiltrate a porous structure. Fe_2O_3 particles in suspension infiltrate and fill pores in the clay particles during heat treatment and contribute to the initiation of crystallisation between iron and clay particles [12]. It has been confirmed in Figure 4(b), where Fe_2O_3 has filled the voids and covered the grain boundaries of clay. A previous study reported that the interparticle contacts, vitrified bridges, and neck contacts in the densification of the sintered material were due to the vitrification with closed and open pores of several sizes, although larger than those observed at lower firing temperatures [20].

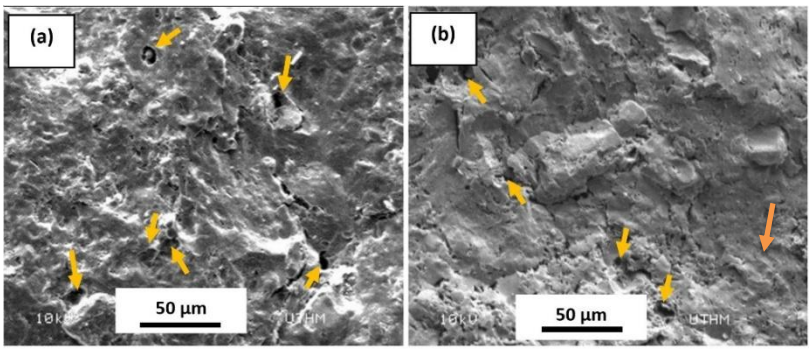

Fig. 4. Microstructure of the samples' fracture surface: (a) clay (CF0); and (b) clay reinforced with 20% Fe_2O_3 (CF20) sintered at 1120 °C. The yellow arrows show the pores exhibited on the fractured surface.

4. Conclusions

Iron (III) Oxide (Fe_2O_3) significantly improves the mechanical performance (MOR) and physical properties (shrinkage) of VCP. The maximum MOR, a robust 45.5 MPa, and shrinkage, 7.93% sintered at 1120 °C, confirm that Fe_2O_3 is a promising sintering additive for clay. The decrease in porosity of clay due to the addition of Fe_2O_3, which is linked to higher MOR and shrinkage, has practical implications. The MOR above 30 MPa and the shrinkage above 5% at the lower sintering temperature, 1050 °C, ascertained in this study, meet the requirements of the vitrified clay pipe (VCP) manufacturing process, making Fe_2O_3 a valuable asset in the VCP industry.

Acknowledgements

The author wishes to acknowledge the appreciation of JPC-Intan Sdn. Bhd. (Claytan Group) for supplying clay materials and communication of this research is made possible through monetary assistance by Universiti Tun Hussein Onn Malaysia and the UTHM Publisher's Office via Publication Fund E15216.

Nomenclatures

a	Width, mm
h	Height, mm
L	Distance between supports of 150 mm
$L1$	Length of sample before sintering, cm
$L2$	Length of sample after sintering, cm
P	The load achieved at the failure time (N)

Greek Symbols

λ	One wavelength of electromagnetic radiation
θ	Semi-vertex angle of the conical nose, rad.

Abbreviations

CAS	Chemical abstract service
CF	Clay and iron percentage
$KAl_2(AlSi_3O_{10})(FOH_2)$	Muscovite
MOR	Modulus of rupture
SEM	Scanning electron microscope
VCP	Vitrified clay pipe
XRD	X-ray diffraction

References

1. Kuliczkowska, E.; Kuliczkowski, A.; and Parka, A. (2022). Damages in vitrified clay sewers in service for 130-142 years. *Engineering Failure Analysis*, 135, 106103.
2. El-Desoky, H.; Farouk, S.; Heikal, M.; El-Mahallawy, M.; and Wahid, A. (2019). Geochemical and technical investigation of some clay materials in the Bahariya Oasis, Western Desert, Egypt: Implication in the vitrified clay pipes industry. *Journal of African Earth Sciences*, 160, 103612.
3. El-Shimy, Y.N.; Amin, S.K.; El-Sherbini, S.A.; and Abadir, M.F. (2014). The use of cullet in the manufacture of vitrified clay pipes. *Construction and Building Materials*, 73, 452-457.
4. Orolínová, Z.; Mockovčiaková, A.; Zeleňák, V.; and Myndyk, M. (2012). Influence of heat treatment on phase transformation of clay-iron oxide composite. *Journal of Alloys and Compounds*, 511(1), 63-69.
5. Dehsheish, H.G.; Karamian, E.; Owsalou, R.G.; Ghasemi-Kahrizsangi, S.; Vefgh, N.; and Soheily, A. (2018). Improvement in performance of MgO-CaO refractory composites by addition of Iron (III) oxide nanoparticles. *Ceramics International*, 44(13), 15880-15886.
6. Pawar, R.R.; Lalhmunsiama; Kim, M.; Kim, J.-G.; Hong, S.-M.; Sawant, S.Y.; and Lee, S.M. (2018). Efficient removal of hazardous lead, cadmium, and arsenic from aqueous environment by iron oxide modified clay-activated carbon composite beads. *Applied Clay Science*, 162, 339-350.
7. Farooq, N.; Khan, M.I.; Shanableh, A.; Qureshi, A.M.; Jabeen, S.; and Rehman, A. (2022). Synthesis and characterization of clay graphene oxide iron oxide (clay/GO/Fe_2O_3)-nanocomposite for adsorptive removal of methylene blue dye from wastewater. *Inorganic Chemistry Communications*, 145, 109956.

8. Xie, T.; Lu, S.; Zeng, J.; Rao, L.; Wang, X.; Wina, M.S.; Zhang, D.; Lu, H.; Liu, X.; and Wang, Q. (2020). Soluble Fe release from iron-bearing clay mineral particles in acid environment and their oxidative potential. *Science of the Total Environment*, 726, 138650.
9. Nie, X.; Xing, X.; Xie, R.; Wang, J.; Yang, S.; Wan, Q.; and Zeng, E.Y. (2023). Impact of iron/aluminum (hydr)oxide and clay minerals on heteroaggregation and transport of nanoplastics in aquatic environment. *Journal of Hazard Materials*, 446, 130649.
10. Liu, Y.; Chen, H.; Sheng, Y.; Hou, W.; Zhang, W.; Hu, W.; and Dong, H. (2025). Abiotic and biotic transformation of petroleum hydrocarbons coupled with redox cycling of structural iron in clay mineral. *Geochimica et Cosmochimica Acta*, 395, 44-63.
11. Tiar, K.; Soualah, A.; Bisio, C.; Marchesi, S.; Pappalardo, V.; Econdi, S.; and Guidotti, M. (2025). Tuning iron loading and specific surface area in iron-containing clays for the oxidative photodegradation of 4-nitrophenol. *Applied Catalysis A: General,* 707, 120522.
12. Guillemin, F.; Duttine, M.; Lecomte-Nana, G.; El Hafiane, Y.; Peyratout, C.; and Smith, A. (2025). Investigation of iron oxide and kaolinite interactions during sintering under controlled atmosphere. *Applied Clay Science*, 276, 107945.
13. Alves, H.P.A.; Silva, J.B.; Campos, L.F.A.; Torres, S.M.; Dutra, R.P.S.; and Macedo, D.A. (2016). Preparation of mullite based ceramics from clay-kaolin waste mixtures. *Ceramics International*, 42(16), 19086-19090.
14. Varela, M.L.; Nascimento, R.M.; Martinelli, A.E.; Hotza, D.; Melo, D.M.; and Melo, M.A.F. (2005). Otimização de uma metodologia para análise mineralógica racional de argilominerais (Optimization of a methodology for rational mineralogical analysis of clay minerals). *Cerâmica*, 51(320), 388-392.
15. González-Miranda, F.M.; Garzón, E.; Reca, J.; Pérez-Villarejo, L.; Martínez-Martínez, S.; and Sánchez-Soto, P.J. (2018). Thermal behaviour of sericite clays as precursors of mullite materials. *Journal of Thermal Analysis and Calorimetry*, 132, 967-977.
16. Khalifa, A.Z.; Cizer, O.; Pontikes, Y.; Heath, A.; Patureau, P.; Bernal, S.A.; and Marsh, A.T.M. (2020). Advances in alkali-activation of clay minerals. *Cement and Concrete Research*, 132, 106050.
17. Rat, E.; Martínez-Martínez, S.; Sánchez-Garrido, J.A.; Pérez-Villarejo, L.; Garzón, E.; and Sánchez-Soto, P.J. (2023). Characterization, thermal and ceramic properties of clays from Alhabia (Almería, Spain). *Ceramics International*, 49, 14814-14825.
18. Semiz, B. (2017). Characteristics of clay-rich raw materials for ceramic applications in Denizli region (Western Anatolia). *Applied Clay Science*, 137, 83-93.
19. Ngun, B.K.; Mohamed, H.; Sulaiman, S.K.; Okada, K.; and Ahmad, Z.A. (2011). Some ceramic properties of clays from central Cambodia. *Applied Clay Science*, 53(1), 33-41.
20. Martínez-Martínez, S.; Pérez-Villarejo, L.; Garzón, E.; and Sánchez-Soto, P.J. (2023). Influence of firing temperature on the ceramic properties of illite-chlorite-calcitic clays. *Ceramics International*, 49(14), Part B, 24541-24557.